Engineered control of genetic variability reveals interplay between quorum sensing, feedback regulation and biochemical noise. Supplementary information.

Yadira Boada[a], Alejandro Vignoni[b], Jesús Picó[a]

[a] *Institut d'Automàtica i Informàtica Industrial, Universitat Politècnica de València, Valencia, Spain*
[b] *Center for Systems Biology Dresden (CSBD), Max Planck Institute of Molecular Cell Biology and Genetics, Pfotenhauerstr. 108, 01307 Dresden, Germany*

S.1. Deterministic model derivation

We first derived a complete biochemical model of the gene synthetic circuit. Then we formulated its corresponding dynamical model based on balance equations and mass-action kinetics. The biochemical reactions considered can be split in two main classes: the *gene expression* reactions, and the *induction* ones. In the *gene expression* block, the main processes considered for each of the proteins were transcription, translation, mRNA degradation and protein degradation. In the *induction* part, the main processes considered were binding between the protein LuxR and the inducer to form the monomer, monomer degradation, dimer formation and its degradation, diffusion of the inducer, inducer degradation, and binding of the dimer to the P_{lux} promoter.

A set of biochemical reactions representing the system are shown in (1)-(2) where the 9 first reactions describe the gene expression, while the remaining reactions represent the diffusion process of AHL and the cell-to-cell communication system, and the degradation of the species. We denoted DNA as the free promoter of *luxI*, $\mathrm{mRNA_{luxI}}$ and $\mathrm{mRNA_{luxR}}$ are the messenger RNA of *luxI* and *luxR* respectively, LuxI, LuxR are proteins, AHL is intracellular inducer and $\mathrm{AHL_{ext}}$ is the extracellular inducer, $\mathrm{V_c = V_{cell}/V_{ext}}$ is the ratio between the cellular and the environment volumes to quantify the AHL or $\mathrm{AHL_{ext}}$ effect considering these two different volumes. The species degradation is denoted as $\emptyset$.

$$
\begin{aligned}
&\xrightarrow{\mathrm{C_R}} \mathrm{mRNA_{luxR}} \\
\mathrm{DNA} &\xrightarrow{\mathrm{k_{eI}}} \mathrm{DNA} + \mathrm{mRNA_{luxI}} \\
\mathrm{mRNA_{luxR}} &\xrightarrow{\mathrm{p_R}} \mathrm{mRNA_{luxR}} + \mathrm{LuxR} \\
\mathrm{mRNA_{luxI}} &\xrightarrow{\mathrm{p_I}} \mathrm{mRNA_{luxI}} + \mathrm{LuxI} \\
\mathrm{LuxI} &\xrightarrow{\mathrm{k_A}} \mathrm{AHL} + \mathrm{LuxI} \\
\mathrm{LuxR} + \mathrm{AHL} &\underset{\mathrm{k_{-1}}}{\overset{\mathrm{k_{-1}/k_{d1}}}{\rightleftarrows}} \mathrm{LuxR \cdot AHL} \\
2(\mathrm{LuxR \cdot AHL}) &\underset{\mathrm{k_{-2}}}{\overset{\mathrm{k_{-2}/k_{d2}}}{\rightleftarrows}} (\mathrm{LuxR \cdot AHL})_2 \\
(\mathrm{LuxR \cdot AHL})_2 + \mathrm{DNA} &\underset{\mathrm{k_{lux}}}{\overset{\mathrm{k_{lux}/k_{dlux}}}{\rightleftarrows}} \mathrm{DNA(LuxR \cdot AHL)_2} \\
\mathrm{DNA(LuxR \cdot AHL)_2} &\xrightarrow{\alpha \mathrm{k_{eI}}} \mathrm{DNA(LuxR \cdot AHL)_2} + \mathrm{mRNA_{luxI}}
\end{aligned}
\tag{1}
$$

Table S1. **Parameters of the gene synthetic circuit model.**

Parameter	Description	Value	Unit	Reference
C_R	Plasmid copy number times LuxR transcription rate	$7.9^{\dagger}$	molecules·min^{-1}	(Boada et al., 2015)
k_{e_I}	LuxI transcription rate	$17.5^{\dagger}$	molecules·min^{-1}	(Boada et al., 2015)
α	Basal expression of *luxI*	0.01		estimated
p_R	Translation rate of mRNA$_{LuxR}$	$10^{\ddagger}$	min^{-1}	(Alon, 2007; Milo et al., 2010)
p_I	Translation rate of mRNA$_{LuxI}$	$3.09^{\ddagger}$	min^{-1}	(Alon, 2007; Milo et al., 2010)
k_A	Synthesis rate of AHL by LuxI	0.04	min^{-1}	(Vignoni et al., 2013)
k_{-1}	Dissociation rate of (LuxR · AHL)	10	min^{-1}	(Weber and Buceta, 2013)
k_{-2}	Dissociation rate of dimer (LuxR · AHL)$_2$	1	min^{-1}	estimated
k_{d1}	Dissociation constant of (LuxR · AHL)	100	molecules	(Urbanowski et al., 2004)
k_{d2}	Dissociation constant of (LuxR · AHL)$_2$	20	molecules	(Harman, 2001)
k_{dlux}	Dissociation constant of (LuxR · AHL)$_2$ to the lux promoter	100	molecules	(Buchler et al., 2005) and refs. therein
d_I	Degradation rate of LuxI	$0.027^{\flat}$	min^{-1}	(Goryachev et al., 2006; Milo et al., 2016)
d_R	Degradation rate of LuxR	$0.2^{\flat}$	min^{-1}	(Boada et al., 2016), and refs. therein
d_A	Degradation rate of AHL	$0.057^{\flat}$	min^{-1}	(Kaufmann et al., 2005; Schaefer et al., 1996)
d_{A_e}	Degradation rate AHL in culture medium	0.04	min^{-1}	(Kaufmann et al., 2005; Schaefer et al., 1996; Kaplan and Greenberg, 1985)
d_{RA}	Degradation rate of (LuxR · AHL)	$0.156^{\flat}$	min^{-1}	(Buchler et al., 2005) and refs. therein
d_{RA_2}	Degradation rate of (LuxR · AHL)$_2$	0.017	min^{-1}	estimated
dm_I	Degradation rate of mRNA$_{LuxI}$	$0.247^{\flat}$	min^{-1}	(Roberts et al., 2006; Santillán and Mackey, 2001)
dm_R	Degradation rate of mRNA$_{LuxR}$	$0.247^{\flat}$	min^{-1}	(Milo et al., 2016; Santillán and Mackey, 2001)
D	Diffusion rate of AHL through the cell membrane	$2^{\P}$	min^{-1}	(Weiss, 1996; Nilsson et al., 2001)
V_{cell}	Typical volume of *E. coli.*	$1.1 \cdot 10^{-9}$	μL/cell	(Milo et al., 2010)
V_{ext}	Typical volume of microfluidic device	$1 \cdot 10^{-3}$	μL	estimated

$$
\begin{aligned}
\mathrm{AHL} &\underset{\mathrm{DV_c}}{\overset{\mathrm{D}}{\rightleftarrows}} \mathrm{AHL_{ext}} \\
\mathrm{mRNA_{luxI}} &\xrightarrow{\mathrm{dm_I}} \emptyset \\
\mathrm{mRNA_{luxR}} &\xrightarrow{\mathrm{dm_R}} \emptyset \\
\mathrm{LuxI} &\xrightarrow{\mathrm{d_I}} \emptyset \\
\mathrm{LuxR} &\xrightarrow{\mathrm{d_R}} \emptyset \\
\mathrm{AHL} &\xrightarrow{\mathrm{d_A}} \emptyset \\
\mathrm{AHL_{ext}} &\xrightarrow{\mathrm{d_{A_e}}} \emptyset \\
\mathrm{LuxR \cdot AHL} &\xrightarrow{\mathrm{d_{RA}}} \emptyset \\
(\mathrm{LuxR \cdot AHL})_2 &\xrightarrow{\mathrm{d_{RA_2}}} \emptyset
\end{aligned}
\tag{2}
$$

The set of reactions (1)-(2) was obtained under the following assumptions:

1. Transcription of genes *luxI* and *luxR* is not reversible, so that k_{e_I} and C_R are the effective transcription rates of LuxI and LuxR respectively,
2. α is the basal expression (leakage) of *luxI*,
3. C_R is the plasmid copy number times the effective constitutive transcription rate of *luxR*,
4. LuxR and AHL binding is a fast and reversible reaction,
5. Dimerization of (LuxR · AHL)$_2$ is a reversible reaction, and
6. The interactions between AHL and AHL$_{ext}$ represent the physical passive diffusion process for cell-to-cell communication via quorum sensing.

The parameter values used in (1)-(2) are listed in the Table S1. Some of these parameters were calculated as follows:

1. The transcription rate k_{e_I} is the minimum LuxI transcription rate. The typical transcription rate in *E. coli.* is $\approx$ 600-6000 bp/min (Alberts et al., 2009). The LuxI length is 582 bp (part BBa_C0161) (Biobrick Foundation, 2006). Therefore, k_{e_I} = (600 bp/min)/582 bp = 1.03 min^{-1},
2. The rate C_R was obtained as the transcription rate obtained as before times the LuxR plasmid copy number. We use the vector pACYC184 with 10 copies/cell, the minimum transcription rate 600 bp/min, and the LuxR length 756 bp (part BBa_C0062) (Biobrick Foundation, 2006). Hence, the plasmid copy number times LuxR transcription rate is $C_R = (10 * 600 \text{ bp/min})/756 \text{ bp} = 7.9$ molecules·min^{-1},

3. The translation rate can be tuned using a ribosome-binding site (RBS) of different strengths. In bacteria, the translation rate is ≈ 30-60 bp/sec (Alberts et al., 2009). Accordingly, the minimum LuxI translations rate is p_I= (1800 bp/min)/582 bp = 3.09 min^{-1}, while the minimum LuxR translations rate is p_R= (1800 bp/min)/756 bp = 2.38 min^{-1},
4. The degradation rates dm_I, dm_R, d_I, d_R, d_A, d_{RA} include the dilution effect due to the cell growth. We considered specific growth rate $\mu_{spe} = 0.017$ min^{-1} corresponding to a cell doubling time of 40 min,
5. The degradation rate $d_{RA_2} = 0.017$ min^{-1} of the transcription factor $(LuxR \cdot AHL)_2$ only depends of the specific growth rate μ_{spe}, assuming $(LuxR \cdot AHL)_2$ is much more stable than the other species in the system (Basu et al., 2005; Buchler et al., 2005),
6. The diffusion coefficient was calculated as $D = \frac{SP_n}{V_{cell}}$ min^{-1}. It depends on the cell surface area $S = 4\pi r^2$ (spherical area with r=10 μm), the membrane permeability $P_n = 3 \cdot 10^{-3} \mu m \cdot min^{-1}$ and the typical *E. coli.* volume $V_{cell} = 1.1 \cdot 10^{-9}$ μL/cell.
7. The dissociation rate of $(LuxR \cdot AHL)_2$ to the lux promoter k_{lux} is not required by the mathematical model, as seen in Section SI S.2.

A dynamical deterministic model corresponding to the biochemical reactions (1)-(2) was obtained using the mass-action kinetics formalism (Alon, 2007; Chellaboina et al., 2009). These kind of models assume the amount of species transformed by the reactions depend solely on the current amount of species, the rates at which these reactions proceed, and the stoichiometry of the reactions (Picó et al., 2015). The resulting deterministic model is given by the set of equations (3-12) representing the dynamics of each species inside the i^{th} cell in a population of N cells. Table S2 describes each state in the dynamical model.

$$\dot{n}_1^i = k_{e_I} n_7^i + \alpha C_I n_8^i - d_{m_I} n_1^i \tag{3}$$
$$\dot{n}_2^i = C_R - d_{m_R} n_2^i \tag{4}$$
$$\dot{n}_3^i = p_I n_1^i - d_I n_3^i \tag{5}$$
$$\dot{n}_4^i = p_R n_2^i + k_{-1} n_5^i - d_R n_4^i - \frac{k_{-1}}{k_{d1}} n_9^i n_4^i \tag{6}$$
$$\dot{n}_5^i = 2k_{-2} n_6^i + \frac{k_{-1}}{k_{d1}} n_9^i n_4^i + \left(-k_{-1} - d_{RA} - 2\frac{k_{-2}}{k_{d2}} n_5^i\right) n_5^i \tag{7}$$
$$\dot{n}_6^i = k_{lux} n_8^i + \frac{k_{-2}}{k_{d2}} {n_5^i}^2 + \left(-k_{-2} - d_{RA_2} - \frac{k_{lux}}{k_{dlux}} n_7^i\right) n_6^i \tag{8}$$
$$\dot{n}_7^i = k_{lux} n_8^i - \frac{k_{lux}}{k_{dlux}} n_6^i n_7^i \tag{9}$$
$$\dot{n}_8^i = -k_{lux} n_8^i + \frac{k_{lux}}{k_{dlux}} n_6^i n_7^i \tag{10}$$
$$\dot{n}_9^i = D\left(\frac{V_{cell}}{V_{ext}} n_{10} - n_9^i\right) - \left(\frac{k_{-1}}{k_{d1}} n_4^i + d_A\right) n_9^i + k_{-1} n_5^i + k_A n_3^i \tag{11}$$
$$\dot{n}_{10} = D\left(-N\frac{V_{cell}}{V_{ext}} n_{10} + \sum_{i=1}^{N} n_9^i\right) - d_{A_e} n_{10} \tag{12}$$

Notice the first two terms in equations (11) and (12) represent the passive diffusion process of AHL and AHL_{ext} molecules, a physical process modeled using a lumped approximation of the Fick's law (Alberts et al., 2009; Weiss, 1996).

S.2. Reduction of the deterministic model.

We carried out model reduction by means of the *Quasi Steady-State Approximation* (QSSA) of the fast chemical species (Mélykúti et al., 2014; Zagaris et al., 2004). In particular, we assumed that binding reactions occur very fast as compared to those corresponding to translation and degradation. Additional algebraic relationships among variables were obtained looking for system invariants (*moieties*).

Conservation laws can be inferred from simple inspection in the model (3-12). Notice the sum of equation (10) representing the variation of free promoter plus equation (11) representing the variation of dimer

Table S2. **Species of the complete model.**

Symbol	Biochemical species	Unit
n_1	Messenger RNA of *luxI*	molecules
n_2	Messenger RNA of *luxR*	molecules
n_3	Protein LuxI	molecules
n_4	Protein LuxR	molecules
n_5	Monomer (LuxR $\cdot$ AHL)	molecules
n_6	Dimer $(\text{LuxR} \cdot \text{AHL})_2$	molecules
n_7	Free promoter DNA	molecules
n_8	Bound promoterDNA$(\text{LuxR} \cdot \text{AHL})_2$	molecules
n_9	Internal inducer AHL	molecules
n_{10}	External inducer AHL_{ext}	molecules

$(\text{LuxR} \cdot \text{AHL})_2$ bound to the promoter is null ($\dot{n}_7^i + \dot{n}_8^i = 0$). This implies that the sum of free and bound promoter is constant ($n_7^i + n_8^i = \text{P}_\text{N}$) and equal to the *plasmid copy number*.

We considered that the RNA polymerase binding/unbinding reactions to the gene promoter proceed much faster than translation and mRNA degradation so they can be assumed to be at quasi-steady state. This is reflected in the values of the reaction rates of equations (4) and (5). Hence, obtained algebraic expressions for $\text{mRNA}_{\text{luxI}}$ (n_1^i) and $\text{mRNA}_{\text{luxR}}$ (n_2^i) using two relationships: $\dot{n}_1^i = 0$ and $\dot{n}_2^i = 0$. Then, these algebraic expressions for n_1 and n_2 can be replaced in equations (6) and (7) respectively. The second QSSA assumption we used concerns the large production of monomer as compared to the dimer one. Thus, we assumed $\dot{n}_5^i = 0$ in equation (8). The resulting expression for the monomer n_5^i can be replaced in equations (7), (9) and (11). All these assumptions lead to the reduced-order model (13-17) for the i^{th} cell in a population of N cells.

$$\dot{n}_1^i = \frac{\text{C}_\text{I}\text{p}_\text{I}}{\text{dm}_\text{I}}\left(\frac{\text{k}_\text{dlux} + \alpha n_3^i}{\text{k}_\text{dlux} + n_3^i}\right) - \text{d}_\text{I} n_1^i \tag{13}$$

$$\dot{n}_2^i = \frac{\text{C}_\text{R}\text{p}_\text{R}}{\text{dm}_\text{R}} + \text{k}_{-1} n_6^i - \left(\frac{\text{k}_{-1}}{\text{k}_\text{d1}} n_4^i + \text{d}_\text{R}\right) n_2^i \tag{14}$$

$$\dot{n}_3^i = \frac{\text{k}_{-2}}{\text{k}_\text{d2}}(n_6^i)^2 - (\text{k}_{-2} + \text{d}_{\text{RA}_2}) n_3^i \tag{15}$$

$$\dot{n}_4^i = \text{k}_{-1} n_6^i + \text{k}_\text{A} n_1^i + \text{D}\left(\frac{\text{V}_\text{cell}}{\text{V}_\text{ext}} n_5 - n_4^i\right) - \left(\frac{\text{k}_{-1}}{\text{k}_\text{d1}} n_2^i + \text{d}_\text{A}\right) n_4^i \tag{16}$$

$$\dot{n}_5 = \text{D}\left(-N\frac{\text{V}_\text{cell}}{\text{V}_\text{ext}} n_5 + \sum_{i=1}^{N} n_4^i\right) - \text{d}_{\text{A}_\text{e}} n_5 \tag{17}$$

with:

$$n_6^i = \frac{\text{k}_\text{d2}(\text{d}_\text{RA} + \text{k}_{-1})}{4\text{k}_2}\left[\sqrt{\frac{8\text{k}_{-2}(2\text{k}_{-2}\text{k}_\text{d1} n_3^i + \text{k}_{-1} n_2^i n_4^i)}{\text{k}_\text{d1}\text{k}_\text{d2}(\text{d}_\text{RA} + \text{k}_{-1})^2} + 1} - 1\right] \tag{18}$$

where all species involved are listed in Table S3. The parameter C_I is the plasmid copy number times LuxI transcription rate. $\text{C}_\text{I} = \text{P}_\text{N} * \text{k}_{\text{e}_\text{I}} = 17.5$ molecules$\cdot$ min^{-1}, where P_N is the LuxI plasmid copy number (vector pBR322 with ≈ 17 copies), and $\text{k}_{\text{e}_\text{I}} = 1.03$ min^{-1} from Table S1. The remaining parameters are the same as those of the full model (see Table S1).

Notice the first term on the right hand side of (13) is a Hill-like function (Alon, 2007). representing the transcription factor regulatory effect (repression in our case) over the expression of protein LuxI.

To validate the reduced model we performed a series of *in silico* experiments. Fig S1 shows some of the results demonstrating the good agreement between the results provided by both the complete and the reduced models. The principal biochemical species LuxI, LuxR and AHL are plotted on the top of Fig S1 for the reduced model (solid line) and the full one (dashed line). The plots of the 5 species eliminated by the reduction ($\text{mRNA}_{\text{luxI}}, \text{mRNA}_{\text{luxR}}$, DNA, DNA$(\text{LuxR} \cdot \text{AHL})_2$ and $(\text{LuxR} \cdot \text{AHL})_2$) were calculated

Table S3. **Species for reduced model.**

Symbol	Biochemical species	Unit
n_1	Protein LuxI	molecules
n_2	Protein LuxR	molecules
n_3	Dimer $(\text{LuxR} \cdot \text{AHL})_2$	molecules
n_4	Internal autoinducer AHL	molecules
n_5	External autoinducer AHL_{ext}	molecules
n_6	Monomer $(\text{LuxR} \cdot \text{AHL})$	molecules

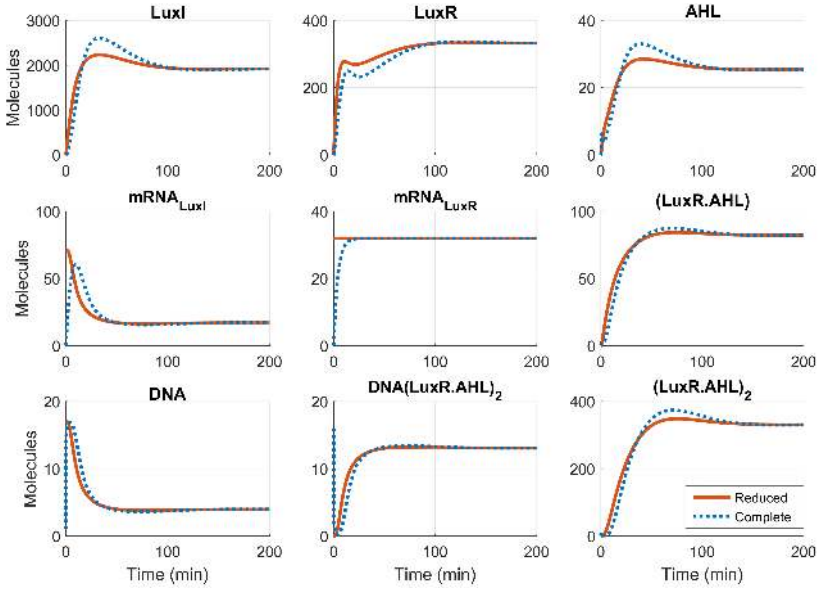

Figure S1. **Validation of the reduced models** Simulation during 250 minutes for a single cell of both the reduced (solid line) and the complete model (dashed line). In both cases the simulations were performed with the same initial conditions and step size: $\delta t = 1 \cdot 10^{-3}$ seconds.

algebraically from the remaining species. The simulation shown was carried over a single cell ($N = 1$). Therefore the amount of molecules of AHL and AHL_{ext} is similar. Hence, the AHL_{ext} plot was omitted in this figure. The agreement between the results of both models was good enough for our purposes, without requiring any *ad hoc* adjustment. From a qualitative point of view, the transient regime of the complete model is similar to the reduced one for all species. The length of the transients and the steady state values coincide in both models.

S.3. Computational analysis

The computational analysis methodology is depicted in figure S2.

S.4. Getting statistical moments and minimising stochastic realizations

The procedure we used to obtain the noise strength from the stochastic simulations is the following:

1. We first ran a simulation with a population of N = 240 cells in a culture volume of $10^{-3}\mu$l, corresponding to an optical cell density OD600 = 0.3, for 400 minutes. From this simulation we obtain 240 time courses corresponding to the protein expression levels in time for each one of the 240 cells in the population.

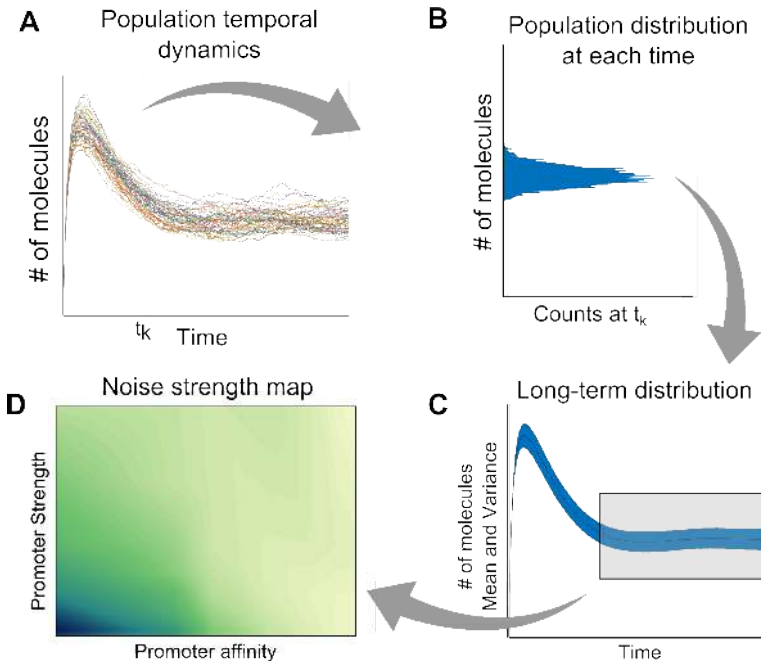

Figure S2. **Methodological procedure to obtain the statistical moments from stochastic simulations of the circuit.** (A) Temporal evolution of one species in the population of cells. (B) Distribution of the number of molecules across the population at each time instant. (C) Acquisition of the long-term distribution for each species. (D) Noise strength map for varying model parameters.

We discarded the first 134 minutes of simulation to ensure the system has reached steady state, using the time samples corresponding to the last 266 minutes (around 100.000 time samples).

2. With these 240 time courses we calculate the mean and the variance across the population at each time instant, obtaining the population mean and variance for each time.
3. Then, using the time-mean across the population, we calculated the temporal mean, thus obtaining a representative of the long-term mean of the protein levels in the population.
4. Finally we calculated the long-term variance by using the law of total variance: the total variance is the sum of the mean of the variance plus the variance of the mean (Weiss, 2006).
5. The noise strength is then calculated with the total mean and total variance of the system. In this way we incorporate and aggregate all the noise (intrinsic) coming from the different cells in the population (extrinsic).

The last two steps were performed to obtain the long-term statistics using only one realization of the simulation, so we reduced the computational burden. We can do this if the system is ergodic, that is, if enough time averaging along one realization is equivalent to getting statistics from many realizations at each time instant. Theoretically proving ergodicity is difficult for our system, so we assessed ergodicity computationally.

We quantified if one realization of the stochastic model for the population of N cells was *enough* to characterize its long-term statistics such as mean, variance and noise strength. Three realizations where performed for each circuit QS/Fb and NoQS/NoFb with the same set of parameters and conditions. We first got the mean across the population for each time instant, for each one of the three realizations. We then selected a portion of the steady state (120 time samples) for each realization. To check whether the realizations are significatively different we performed a Kruskal-Wallis Test (Kruskal and Wallis, 1952) on them. For the NoQS/NoFb network in Fig S3Top, the results of the Kruskal-Wallis analysis shows there is no statistically significance to reject the hypothesis of the three realizations having the same LuxI's median and noise strength $\eta^2_{LuxI} = 0.1307$, with $[Test - statistic, P - value] = [0.0018, 0.9991]$. The same conclusion is shown in Fig S3Bottom for the QS/Fb network with $[Test - statistic, P - value] = [0.0006, 0.980714]$.

We obtained P-values greater than 0.05, indicating there is no statistically significant difference with 95.0 % confidence level, confirming the system is ergodic. Therefore, one realization of the population of N interconnected cells for the NoQS/NoFb or the QS/Fb network, provided sufficient simulated time length to perform the time average, is enough to obtain representatives of the long-term moments of the population.

In order to visually show the similarity between realizations, Fig S3 shows the LuxI distributions of the three realizations in both circuits. The LuxI long-term distributions were unimodal and well shaped.

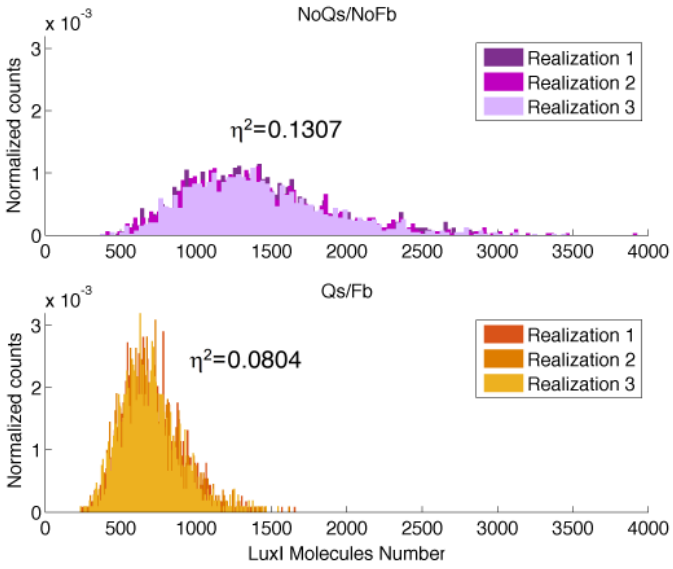

Figure S3. **Different realizations, similar statistics moments.** Population histograms of the LuxI molecules number for three different realizations of the NoQS/NoFb (top), and QS/Fb (bottom) circuits.

S.5. Validation of the non-linear propensities

Usually the stochastic algorithms treat all reaction events alike. Thus they use most of its time simulating the many relatively uninteresting fast reaction events instead of explicitly simulating only the slow reactions. Yet, slow reactions dependency on the fast ones can be approximated using different approaches (e.g. QSSA). Then, they can be treated as new deterministic or stochastic rational slow reactions. This approximation leads to higher-order propensity functions. The use of these higher-order terms in stochastic simulation is justified in many cases (Cao et al., 2005; Rao and Arkin, 2003).

In our case, the propensity function $f(n_3^i, t)$ (see Methods, Mathematical model) represents the Hill-like function of gene expression for protein LuxI in the i^th cell. This propensity function resulted from the model reduction, so that the propensity term $f(n_3^i, t)$ contains all fast interactions between the *luxI* promoter (DNA), $\mathrm{mRNA_{luxI}}$ and the repressor $(\mathrm{LuxR \cdot AHL})_2$ repeated again in (19).

$$
\begin{aligned}
\mathrm{DNA} &\xrightarrow{\mathrm{C_I}} DNA + \mathrm{mRNA_{luxI}} \\
(\mathrm{LuxR \cdot AHL})_2 + \mathrm{DNA} &\underset{\mathrm{k_{lux}}}{\overset{\mathrm{k_{lux}/k_{dlux}}}{\rightleftarrows}} \mathrm{DNA(LuxR \cdot AHL)_2} \\
\mathrm{DNA(LuxR \cdot AHL)_2} &\xrightarrow{\alpha \mathrm{C_I}} \mathrm{DNA(LuxR \cdot AHL)_2} + \mathrm{mRNA_{luxI}} \\
\mathrm{mRNA_{luxI}} &\xrightarrow{\mathrm{dm_I}} \emptyset
\end{aligned}
\tag{19}
$$

The set of reactions in (19) were approximated (see section S.2) as the two equivalent reactions:

$$\begin{gathered}(\mathrm{LuxR}\cdot\mathrm{AHL})_2 \xrightarrow{f(n_3,t)} (\mathrm{LuxR}\cdot\mathrm{AHL})_2 + \mathrm{mRNA_{luxI}} \\ \mathrm{mRNA_{luxI}} \xrightarrow{\mathrm{dm_I}} \emptyset\end{gathered} \tag{20}$$

where $f(n_3^i,t) \triangleq \frac{\mathrm{C_I p_I}}{\mathrm{dm_I}}\left(\frac{\mathrm{k_{dlux}}+\alpha n_3^i}{\mathrm{k_{dlux}}+n_3^i}\right)$ describes the $\mathrm{mRNA_{luxI}}$ transcription in an equivalent way to (19), and n_3^i is the transcription factor $(\mathrm{LuxR}\cdot\mathrm{AHL})_2$ for the i^{th} cell.

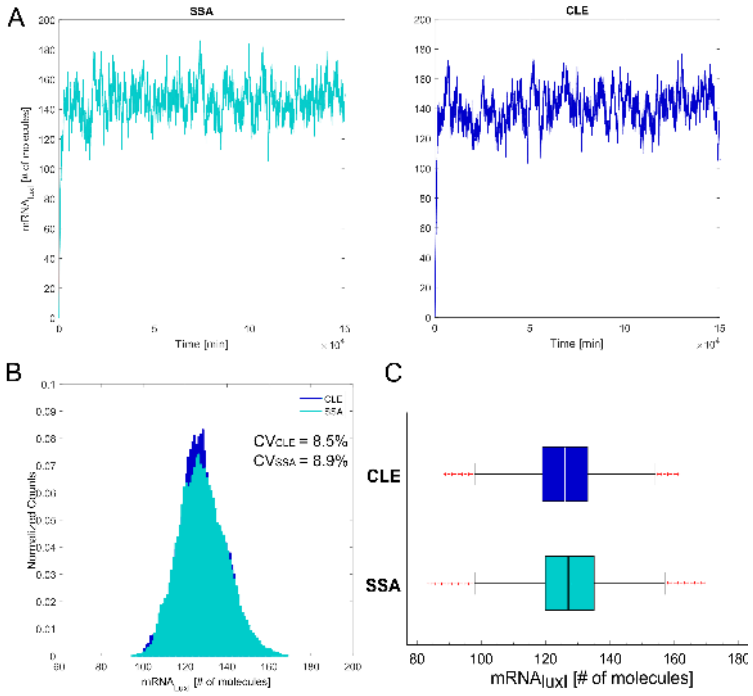

Figure S4. **SSA and CLE comparison validate use of propensity functions.** (A) One realization of $\mathrm{mRNA_{luxI}}$ made using the SSA (cyan color) and the CLE (blue color) respectively. Both trajectories match during a large temporal window ($15{\cdot}10^4$ min). (B) Histogramsshow close means and covariances. (C) Box-and-Whisker plots showing both medians $\widetilde{\mathrm{SSA}} = 127.7$ molecules, and $\widetilde{\mathrm{CLE}} = 126.1$ molecules are statistically indistinguishable

To validate the use of the propensity function $f(n_3^i,t)$, we simulated the reactions (20) using the CLE, and the reactions (19) using the SSA (Gillespie direct method), for one single-cell under the same conditions.

The SSA trajectory, plotted in Fig S4A (left), matched very well with the CLE trajectory shown in Fig S4A (right) during the whole simulation. For both trajectories (SSA and CLE respectively), we obtained similar distributions and no meaningful differences between their first statistical moments: $\mu_{SSA} \approx \mu_{CLE}$ molecules, and $\sigma_{SSA} \approx \sigma_{CLE}$, as shown in Fig S4B. In turn, noise strength of $\mathrm{mRNA_{luxI}}$ in both SSA and CLE trajectories had similar values ($\eta^2_{SSA} = 0.008$, $\eta^2_{CLE} = 0.0072$).

Fig S4C shows the Box-and-Whisker plots of the realizations. Their medians $\widetilde{CLE}$ (white line), and $\widetilde{SSA}$ (black line) are practically the same, accordingly with the Kruskal-Wallis Test which reveals there is no statistically significant difference between their medians with a 95.0 % confidence level ($[Test-statistic,\ P-value] = [-2.09067\cdot 10^6,\ 1.0]$).

S.6. Effect of population size and cell density

The optical density (OD) of a cell culture depends on the number of cells, and the volume of the culture. In our computational simulations we selected the number N of cells and the volume V_{ext} to obtain different OD_{600} values using the relationship:

$$OD = N\frac{1}{V_{ext}} * \frac{1}{N_{OD|1}} \tag{21}$$

where N is the number of cells ($N = 240$ bringing the OD_{600} to 0.3), $V_{ext} = 1 \cdot 10^{-3}\ \mu L$, and $N_{OD|1} = 8 \cdot 10^5$ is the quantity of cells contained in 1 μL of bacterial culture when the OD_{600} is 1 (*Source:* **Agilent**, *E. coli* Cell Culture Concentration from OD_{600} Calculator).

In order to see whether quorum sensing effect on our circuit depends on the cell density, we changed the OD as a function of the number of cells and the volume. Fig S5A shows the LuxI noise strength obtained at different values of OD ranging from 0.005 to 5. First, we kept the number of cells constant ($N = 240$ cells) and changed the culture volume V_{ext} from 0.06 to 0.0003 μL (blue squares). The OD ratio is tabulated in Table S4. Next, we changed the cell number N and the external volume V_{ext} simultaneously, so as to have volumes in more realistic range for microfluidic settings (green squares). Their values (see Table S4) were chosen trying to keep the same cell densities as in the first case.

Table S4. **OD changing the cell number and volume.**

Cell number fixed						
N (cells)	240	240	240	240	240	240
V_{ext} (μL)	0.06	0.03	0.006	0.003	0.0006	0.0003
OD_{600}	0.005	0.01	0.05	0.1	0.5	1
Cell number and external volume are variable						
N (cells)	240	240	1200	2400	4800	12000
V_{ext} (μL)	0.03	0.006	0.015	0.006	0.006	0.003
OD_{600}	0.01	0.05	0.1	0.5	1	5

Table S5. **OD fixed.**

N (cells)	240	1200	2400	4800	12000
V_{ext} (μL)	0.001	0.005	0.01	0.02	0.05
OD_{600}	0.3	0.3	0.3	0.3	0.3

Moreover, to evaluate how representative of a cell population is a simulation with $N = 240$ cells, we changed the number of cells and the volume to achieve a constant cell density at different cell numbers. The cell numbers and volumes used in this case are in the intervals: $N = [240,\ 12000]$ cells and $V_{ext} = [0.001,\ 0.05]\mu L$ (see Table S5). Figure S5B shows the LuxI noise strength for different values of N ranging from 240 cells to 12000 cells. In all cases LuxI noise strength did not appreciably change.

S.7. LuxR Parameters variation

We sampled the LuxI expression parameters in the ranges of $k_{dlux} = [10 - 2000]$ nM, $\alpha = [0.01 - 0.1]$, and $p_I = [0.2 - 10]\ \mathrm{min}^{-1}$, together with the LuxR parameters in the ranges of $d_R = [0.02 - 0.2]\,\mathrm{min}^{-1}$, and $p_R = [0.2 - 10]\ \mathrm{min}^{-1}$. The simulation results are showed in Fig S6. In the top panel, $d_R = 0.02\,\mathrm{min}^{-1}$ and the different colors code for several values of p_R. The same, for the central panel with $d_R = 0.07\,\mathrm{min}^{-1}$ and the bottom panel $d_R = 0.2\,\mathrm{min}^{-1}$.

S.8. Plasmids and experimental conditions

All plasmids are shown in Figures S7-S9.

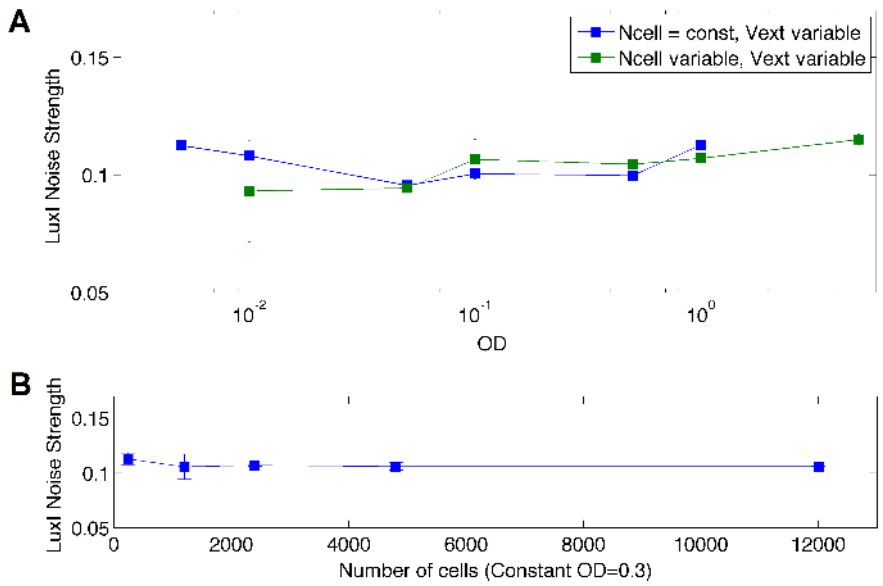

Figure S5. **LuxI noise strength comparison at different OD_{600} values**. (A) LuxI noise strength does not appreciably change for different OD= [0.005, 0.01, 0.05, 0.1, 0.5, 1, 5], obtained either changing only the volume and keeping the cell number constant in N=240 (blue squares) or when changing both the cells number together with the volume (green squares). (B) LuxI noise strength for different number of cells and volume, but keeping constant $OD_{600} = 0.3$.

S.9. Experimental flow cytometry protocol

These protocols were performed over two consecutive days for each experiment in order to measure the activity of the output protein LuxI in both QS/Fb and NoQS/NoFb circuits. The protocols were adapted from Olson et al. (2014).

QS/Fb, NoQS/NoFb growth and induction via flow cytometry protocol.

1. Start a 37 °C, shaking overnight culture from a -80 °C stock in a tube containing 3 mL LB medium and the appropriate antibiotics (100 μg/mL ampicillin, 12.5 μg/mL tetracycline and 34 μg/mL chloramphenicol for both QS/Fb and NoQS/NoFb systems in 14 mL culture tubes).
2. After the overnight culture has grown for 12-16 h, prepare M9 medium (200 mL is made with: 151.58 mL autoclaved, distilled H2O, 40 mL 5x M9 salts, 4 mL 10 % casamino acids, 4 mL 20 % glucose, 400 μL 1 M MgSO4, 20 μL CaCl2). Add appropriate antibiotics to medium and stir the container to ensure the antibiotics are mixed well in the medium.
3. Measure the OD_{600} of the overnight culture.
4. Dilute the overnight culture into the M9 + antibiotics, bringing the OD_{600} to 0.004. Shake the container to ensure the cells are mixed well in the medium.
5. Distribute 3 mL of inoculated medium into each 8 BD Falcon round-bottom 14 mL polypropylene test tubes (BD Biosciences Catalog Number 352006).
6. Incubate tubes at 37 °C with shaking at 250 rpm for 3 h.
7. Dilute 5 mg of AHL (N-3-Oxohexanoyl-L-homoserine lactone, Santa Cruz Biotecnology Catalog Number SC205396) into 468.98 μL of DMSO to reach a solution 50 mM. This stock was stored at -20 °C until use.
8. Successively dilute AHL 50 mM into M9 reaching different AHL concentrations to induce the culture tubes. Take into account the final desired AHL concentration and the total test tube volume. We induce AHL 10 and 50 nM to measure final repression levels Egland and Greenberg (2000).

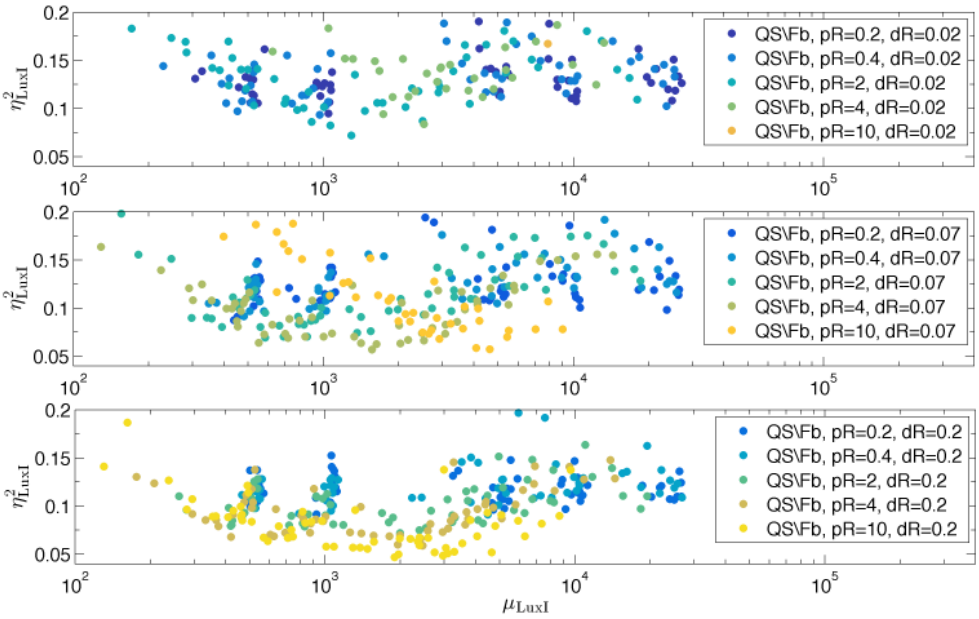

Figure S6. **LuxI noise strength *vs.* LuxI mean.** Increasing the LuxR turnover as a function of the degradation rate attenuates LuxI noise strength: $d_R = 0.02\,\mathrm{min}^{-1}$ (top panel). $d_R = 0.07\,\mathrm{min}^{-1}$ (central panel). $d_R = 0.2\,\mathrm{min}^{-1}$ (bottom panel).

9. After 2 h of growth, quickly induce the test tubes at AHL 0, 10 and 50 nM.
10. Incubate tubes at 37 °C with shaking at 250 rpm for 4 h.
11. After 4 h of induction and growth, harvest all test tubes by immediately transferring them into an ice-water bath. Wait 10 min for the cultures to equilibrate to the cold temperature and for gene expression to stop.
12. Prepare a solution of phosphate-buffered saline (PBS: 137 mM NaCl, 2.7 mM KCl, 10 mM Na2HPO4, 2 mM KH2PO4, pH to 7.4) + 500 μg/mL of the transcription inhibitor rifampicin (Rif, Tokyo Chemical Industry, cat. ♯R0079). Prepare at least 1 mL for each culture tube to be measured via flow cytometry. Rif dissolves slowly, so allow 45 - 60 min of stirring. Also at this time, begin preparing a 37 °C water bath.
13. Filter the dissolved solution of PBS + Rif through a 0.22-μm 20-mL syringe filter.
14. Transfer 1 mL of the filtered PBS + Rif into one 5 mL cytometer tube per culture sample, and chill tubes in an ice-water bath.
15. Transfer 50 μL of each chilled culture from step 7 into the chilled PBS + Rif solution.
16. Incubate the PBS + Rif + culture tubes in a 37 °C water bath for 1 h.
17. Transfer the tubes back into ice-water bath.
18. Wait 15 min, and then begin measuring each tube on a flow cytometer.

Flow cytometry data acquisition. Cytometry acquisition and analysis was performed using a BD FACSCalibur (Serie Nr. E14600085) flow cytometer with the laser system blue (488 nm) and red (635 nm). The FL1 (GFPmut3b) acquisition channel has a 510/21-nm emission filter. Acquisition was performed with typical count rates of 1,000-2,000 events/sec. Approximately 50,000 events were stored for each sample. After acquisition performed with CellQuest Pro 5.2.1 software, the raw cytometry data were processed using the custom-made Matlab scripts described in section S.11.

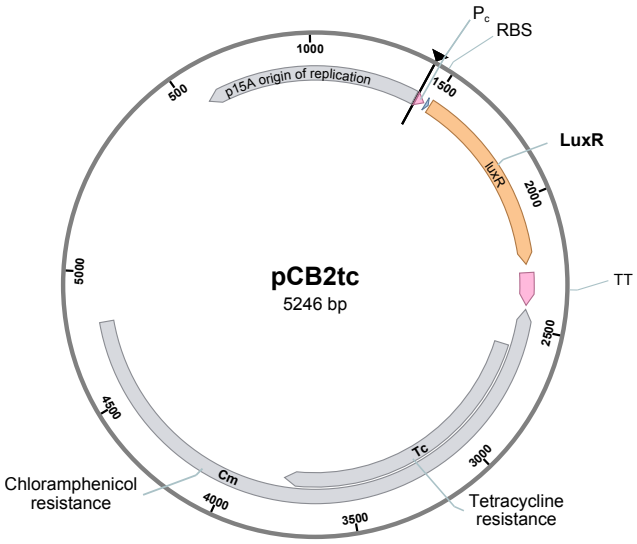

Figure S7. **Plasmid pCB2tc**

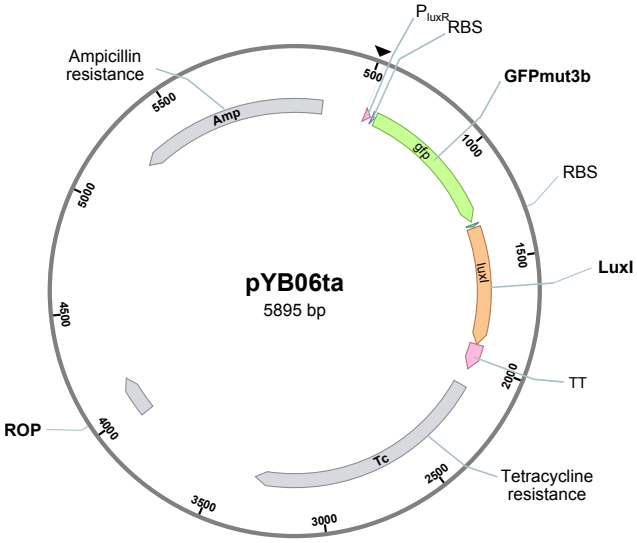

Figure S8. **Plasmid pYB06ta**

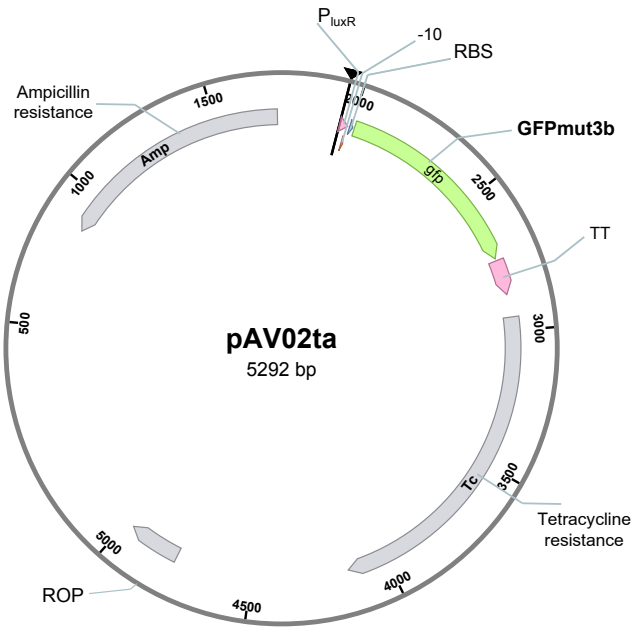

Figure S9. **Plasmid pAV02ta**

S.10. Comparison between flow cytometry experimental data and computational simulations

Data from flow cytometry were processed with our scripts (see SI Section S.11). First, cytometry data were read using the ***fca_readfcs*** Matlab function. Then, the first 250 and last 100 events were removed from the data set to avoid transient errors introduced owing to uneven pressurization of the sample tube. After this, the highest and lowest measured histogram channel for each of the measured values (FSC, SSC, and FL1) were removed, as the events in these channels have an undetermined fluorescence value. All this was done using the ***trim*** Matlab function. Next, the 2D binning of FSC and SSC was performed together with a smooth representation of the 2D histogram using the function ***smoothing***, shown in Fig. S10A. The fluorescence histogram from FL1 raw data, corresponding to the all this events is plotted in Fig. S10B. From this, the normalized and smoothed representation of the histogram was used to obtain contour level curves. Then, it is possible to use them as gate to select the events that are enclosed by the desired contour level using the function ***contour_gating***. This contour level curve was used to isolate a uniformly sized population of cells, and it is naturally aligned with the observed cell population. The gating procedure leaves $N = 15000 - 20000$ events shin in Fig. S10C. This events were then scaled back to linear (detectors were set to log scale) using the parameters from the header of the FCS file. Next, a trim was performed on FL1 to remove a small number of apparent noncellular events with very low and very high fluorescence, the fluorescence corresponding to the gated events is shown in Fig. S10D. Finally experimental data were multiplied by a scale factor of 2.72 to obtain the histograms shown in Figure S11 and in Figure 1C panel left in the main text. Figure S11 shows the overlays of experimental flow cytometry with the simulation results for the QS/Fb circuit in panel A and the NoQS/NoFb in panel B. Simulation results are shown in colored bars and experimental results are black lines overlay.

S.11. Matlab and OpenFPM CODE

A short description of the main functions integrating the code used to simulate the model and process experimental data is given below. It has been divided in three groups: files related to parameters setting (Matlab), files to simulate the model (OpenFPM client in C++), and files used to process experimental data

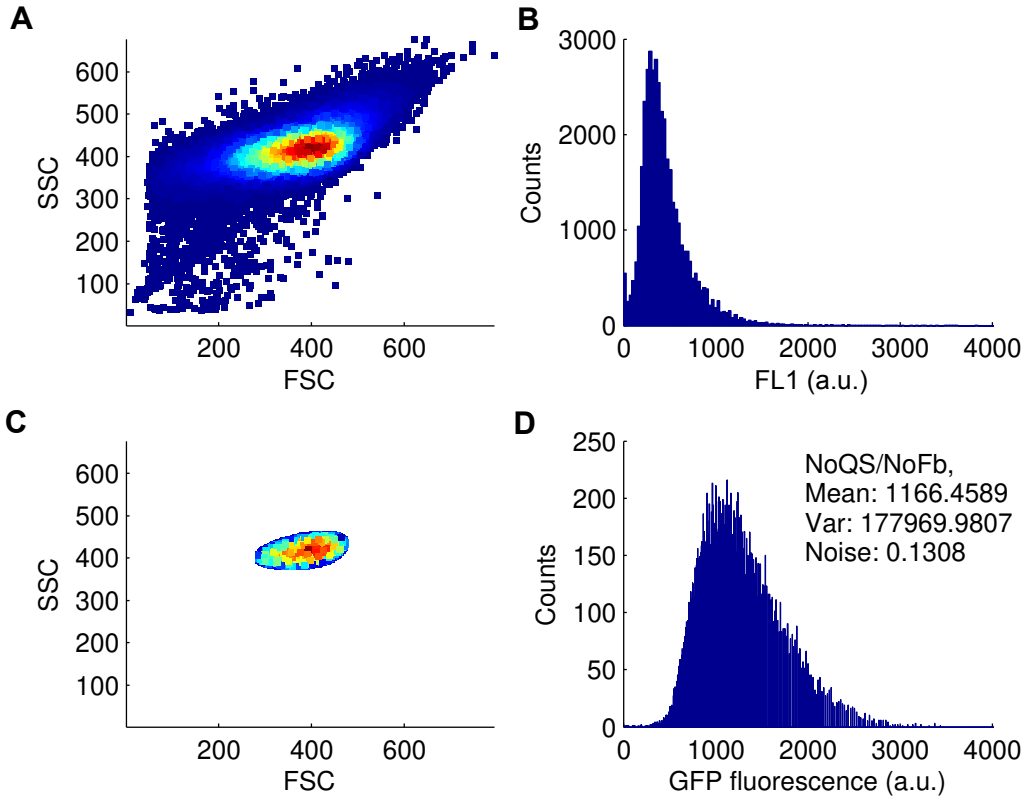

Figure S10. **Flow cytometry experimental data postprocessing.** (A) Forward scatter vs. side scatter plot of the raw data. Colormap show numbers of events (from low in blue to high in dark red). (B) Fluorescence histogram from FL1 raw data, corresponding to the events plotted in panel A. (C) Forward scatter vs. side scatter plot showing the contour gated events. (D) Fluorescence histogram corresponding to the gated events plotted in panel C.

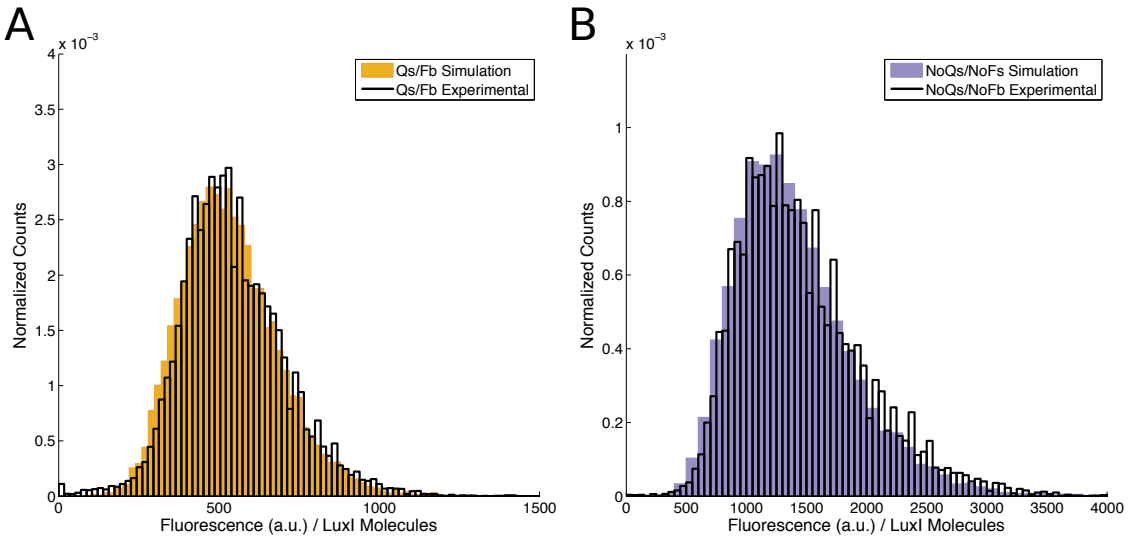

Figure S11. **Comparison between flow cytometry experimental data and computational simulations.** Overlays of experimental flow cytometry with the simulation results. (A) QS/Fb circuit. (B) NoQS/NoFb circuit. Simulation results are shown in colored bars. Experimental results are shown as black lines overlay.

from flow cytometry (Matlab). All them can be downloaded from `http://sb2cl.ai2.upv.es/content/software`.

The stochastic simulation of our synthetic circuit is implemented using *langevin*, an OpenFPM client in C++. Information about OpenFPM installation can be found in its webpage `http://openfpm.mpi-cbg.de/`. The best option for a system that is natively supported (i.e. Linux based systems, Mac, etc.) is to run the code:

```
clone https://github.com/incardon/openfpm_pdata.git && cd openfpm_pdata && ./install
```

and follow the installation instructions therein.

C++ code - OpenFPM client

- ***main.cpp*** is the OpenFPM client *langevin* code. It implements the main body and two auxiliary functions. The first function opens the file param.dat created by the Matlab script and sets the parameters values for each cell. The second function is called at each simulation time step to update the system states (number of molecules of species) using the Euler-Maruyama algorithm.
- ***Makefile*** has the information for *make* to compile the C++ source code.
- ***langevin.mk*** has the information for *Makefile* to obtain all the paths and libraries. Should be replaced by the *example.mk* file generated by the OpenFPM instalation.

Computational cost Execution of 120 parameter sets takes around 20 minutes when performed in a Intel XEON Server with 8 cores and 32 Gb of RAM Memory.

Model code - Parameter setting

- ***Evaluate_CLE_Extrinsic.m*** is a script to set the parameters for the model and run the *langevin* OpenFPM client. It generates a matrix with all required parameters,runs *langevin* and saves the results obtained both as a variable in the Matlab workspace and as a Matlab .mat file.
- ***struct2csv_append.m*** is a function to convert a Matlab structure into a csv file that can be open with the *langevin* OpenFPM client.

Model code - Flow cytometry data postprocessing

- ***plot_tubes.m*** is the main script used to read, trim, smooth and gate the data. It plots the FSC vs SSC scatter and the FL1 histogram before and after the gating procedure. Then it calculates the mean and noise strength of the gated data.
- ***fca_readfcs.m*** is a function obtained from Matlab Central (`www.mathworks.com/matlabcentral/fileexchange/9608-fcs-data-reader`) by Laszlo Balkay. The function reads the raw data and returns the header of the file with information about the acquisition and the raw data (FSC, SSC, FL1).
- ***trim.m*** is a function that trims the raw data. First, the first 250 and last 100 events are removed from the data set to avoid transient errors introduced owing to uneven pressurization of the sample tube. Then each channel is trimmed to the user defined limits. In general this limits are the highest and lowest measured histogram channel for each of the measured values (FSC, SSC, and FL1), as these events have an undetermined fluorescence value.
- ***smoothing.m*** is a function that binds the 2D (FSC,SSC) raw data and returns a smoothed version of the 2D histogram.
- ***contour_gating.m*** is a function that gates FSC and SSC data based on the contour obtained from *smoothing.m*. The user can select the contour level. Then all the events inside the contour are gated in.

References

Alberts, B., Bray, D., Hopkin, K., Johnson, A. D., Johnson, A., Roberts, K., Lewis, J., Raff, M., Walter, P., 2009. Essential Cell Biology, 3rd Edition. Garland Science.

Alon, U., 2007. An Introduction to Systems Biology. Desing Principles of Biological Circuits. Champan and Hall/CRC, Edition.

Basu, S., Gerchman, Y., Collins, C. H., Arnold, F. H., Weiss, R., 4 2005. A synthetic multicellular system for programmed pattern formation. Nature 434 (7037), 1130–4.

Biobrick Foundation, 2006. Part registry [online]. `http://partsregistry.org/`, accesed: 20/02/2015.

Boada, Y., Reynoso-Meza, G., Picó, J., Vignoni, A., 2016. Multi-objective optimization framework to obtain model-based guidelines for tuning biological synthetic devices: an adaptive network case. BMC Syst Biol 10 (1), 27.

Boada, Y., Vignoni, A., Navarro, J. L., J.Picó, 2015. Improvement of a cle stochastic simulation of gene synthetic network with quorum sensing and feedback in a cell population. Proceedings 14th annual European Control Conference.

Buchler, N. E., Gerland, U., Hwa, T., 2005. Nonlinear protein degradation and the function of genetic circuits. Proceedings of the National Academy of Sciences of the United States of America 102 (27), 9559–9564.

Cao, Y., Gillespie, D. T., Petzold, L. R., 2005. The slow-scale stochastic simulation algorithm. The Journal of chemical physics 122 (1), 014116.

Chellaboina, V., Bhat, S., Haddad, W., Bernstein, D., 8 2009. Modeling and analysis of mass-action kinetics. IEEE Control Systems Magazine 29 (4), 60–78.

Egland, K. A., Greenberg, E. P., 2000. Conversion of the vibrio fischeri transcriptional activator, luxr, to a repressor. Journal of Bacteriology 182 (3), 805–811.

Goryachev, A. B., Toh, D. J., Lee, T., 2006. Systems analysis of a quorum sensing network: design constraints imposed by the functional requirements, network topology and kinetic constants. Biosystems 83 (2-3), 178–87.

Harman, J. G., 2001. Allosteric regulation of the camp receptor protein. Biochimica et Biophysica Acta (BBA)-Protein Structure and Molecular Enzymology 1547 (1), 1–17.

Kaplan, H. B., Greenberg, E. P., 1985. Diffusion of autoinducer is involved in regulation of the vibrio fischeri luminescence system. Journal of bacteriology 163 (3), 1210–1214.

Kaufmann, G. F., Sartorio, R., Lee, S.-H., Rogers, C. J., Meijler, M. M., Moss, J. A., Clapham, B., Brogan, A. P., Dickerson, T. J., Janda, K. D., 2005. Revisiting quorum sensing: discovery of additional chemical and biological functions for 3-oxo-n-acylhomoserine lactones. Proceedings of the National Academy of Sciences of the United States of America 102 (2), 309–314.

Kruskal, W. H., Wallis, W. A., 1952. Use of ranks in one-criterion variance analysis. Journal of the American statistical Association 47 (260), 583–621.

Mélykúti, B., Hespanha, J. a. P., Khammash, M., 8 2014. Equilibrium distributions of simple biochemical reaction systems for time-scale separation in stochastic reaction networks. J R Soc Interface 11 (97), 20140054.

Milo, R., Phillips, R., Orme, N., 2016. Cell Biology by the Numbers. Garland Science.

Milo et al., R., 2010. B10numb3r5, the database of useful biological numbers. http://bionumbers.hms.harvard.edu/. Web page.

Nilsson, P., Olofsson, A., Fagerlind, M., Fagerström, T., Rice, S., Kjelleberg, S., Steinberg, P., 2001. Kinetics of the ahl regulatory system in a model biofilm system: how many bacteria constitute a quorum? Journal of molecular biology 309 (3), 631–640.

Olson, E. J., Hartsough, L. A., Landry, B. P., Shroff, R., Tabor, J. J., 2014. Characterizing bacterial gene circuit dynamics with optically programmed gene expression signals. Nature methods 11 (4), 449–455.

Picó, J., Vignoni, A., Picó-Marco, E., Boada, Y., 7 2015. Modelling biochemical systems: from mass action kinetics to linear noise approximation. Revista Iberoamericana de Automática e Informática Industrial RIAI 12 (3), 241–252.

Rao, C. V., Arkin, A. P., 2003. Stochastic chemical kinetics and the quasi-steady-state assumption: application to the gillespie algorithm. The Journal of chemical physics 118 (11), 4999–5010.

Roberts, C., Anderson, K. L., Murphy, E., Projan, S. J., Mounts, W., Hurlburt, B., Smeltzer, M., Overbeek, R., Disz, T., Dunman, P. M., 2006. Characterizing the effect of the staphylococcus aureus virulence factor regulator, sara, on log-phase mrna half-lives. Journal of bacteriology 188 (7), 2593–2603.

Santillán, M., Mackey, M. C., 2001. Dynamic regulation of the tryptophan operon: A modeling study and comparison with experimental data. Proceedings of the National Academy of Sciences 98 (4), 1364–1369.

Schaefer, A. L., Val, D. L., Hanzelka, B. L., Cronan, J. E., Greenberg, E. P., 1996. Generation of cell-to-cell signals in quorum sensing: acyl homoserine lactone synthase activity of a purified vibrio fischeri luxi protein. Proceedings of the National Academy of Sciences 93 (18), 9505–9509.

Urbanowski, M. L., Lostroh, C. P., Greenberg, E. P., 1 2004. Reversible acyl-homoserine lactone binding to purified vibrio fischeri luxr protein. Journal of Bacteriology 186 (3), 631–637.

Vignoni, A., Oyarzún, D. A., Picó, J., Stan, G. B., 2013. Control of protein concentrations in heterogeneous cell populations. In: 2013 European Control Conference (ECC). pp. 3633–3639.

Weber, M., Buceta, J., 2013. Dynamics of the quorum sensing switch: stochastic and non-stationary effects. BMC Syst Biol 7, 6.

Weiss, N. A., 2006. A course in probability. Addison-Wesley.

Weiss, T. F., 1996. Cellular biophysics. Vol. 1. MIT press Cambridge, Mass:.

Zagaris, A., Kaper, H. G., Kaper, T. J., 2004. Analysis of the computational singular perturbation reduction method for chemical kinetics. Journal of Nonlinear Science 14 (1), 59–91.